



In situ 3D characterization of historical coatings and wood using multimodal nonlinear optical microscopy

Gaël Latour, Jean-Philippe Echard, Marie Didier, Marie-Claire Schanne-Klein

► To cite this version:

Gaël Latour, Jean-Philippe Echard, Marie Didier, Marie-Claire Schanne-Klein. In situ 3D characterization of historical coatings and wood using multimodal nonlinear optical microscopy. *Optics Express*, 2012, 20 (22), pp.24623-24635. 10.1364/OE.20.024623 . hal-00123067

HAL Id: hal-00123067

<https://hal.science/hal-00123067v1>

Submitted on 9 May 2014

HAL is a multi-disciplinary open access archive for the deposit and dissemination of scientific research documents, whether they are published or not. The documents may come from teaching and research institutions in France or abroad, or from public or private research centers.

L'archive ouverte pluridisciplinaire **HAL**, est destinée au dépôt et à la diffusion de documents scientifiques de niveau recherche, publiés ou non, émanant des établissements d'enseignement et de recherche français ou étrangers, des laboratoires publics ou privés.

In situ 3D characterization of historical coatings and wood using multimodal nonlinear optical microscopy

Gaël Latour,^{1,*} Jean-Philippe Echard,² Marie Didier,² and Marie-Claire Schanne-Klein¹

¹Laboratory for Optics and Biosciences, Ecole Polytechnique, CNRS, INSERM U696, F-91128, Palaiseau, France

²Laboratoire de recherche et de restauration, Musée de la musique, Cité de la musique, 221 avenue Jean-Jaurès, F-75019, Paris, France

*gael.latour@polytechnique.edu

Abstract: We demonstrate multimodal nonlinear optical imaging of historical artifacts by combining Second Harmonic Generation (SHG) and Two-Photon Excited Fluorescence (2PEF) microscopies. We first identify the nonlinear optical response of materials commonly encountered in coatings of cultural heritage artifacts by analyzing one- and multi-layered model samples. We observe 2PEF signals from cochineal lake and sandarac and show that pigments and varnish films can be discriminated by exploiting their different emission spectral ranges as in luminescence linear spectroscopy. We then demonstrate SHG imaging of a filler, plaster, composed of bassanite particles which exhibit a non centrosymmetric crystal structure. We also show that SHG/2PEF imaging enables the visualization of wood microstructure through typically 60 μm -thick coatings by revealing crystalline cellulose (SHG signal) and lignin (2PEF signal) in the wood cell walls. Finally, *in situ* multimodal nonlinear imaging is demonstrated in a historical violin. SHG/2PEF imaging thus appears as a promising non-destructive and contactless tool for *in situ* 3D investigation of historical coatings and more generally for wood characterization and coating analysis at micrometer scale.

©2012 Optical Society of America

OCIS codes: (180.4315) Nonlinear microscopy; (300.6280) Spectroscopy, fluorescence and luminescence; (310.3840) Materials and process characterization; (190.4180) Multiphoton processes; (180.6900) Three-dimensional microscopy.

References and links

1. N. Gierlinger and M. Schwanninger, "Chemical imaging of poplar wood cell walls by confocal Raman microscopy," *Plant Physiol.* **140**(4), 1246–1254 (2006).
2. G. Latour, J.-P. Echard, B. Soulier, I. Emond, S. Vaiedelich, and M. Elias, "Structural and optical properties of wood and wood finishes studied using optical coherence tomography: application to an 18th century Italian violin," *Appl. Opt.* **48**(33), 6485–6491 (2009).
3. P. Targowski and M. Iwanicka, "Optical coherence tomography: its role in the non-invasive structural examination and conservation of cultural heritage objects—a review," *Appl. Phys. A Mater. Sci. Process.* **106**(2), 265–277 (2012).
4. G. Latour, G. Georges, L. Siozade, C. Deumie, and J.-P. Echard, "Study of varnish layers with optical coherence tomography in both visible and infrared domains," *Proc. SPIE* **7391**, 73910J, 73910J-7 (2009).
5. G. Latour, J. Moreau, M. Elias, and J.-M. Frigerio, "Micro-spectrometry in the visible range with full-field optical coherence tomography for single absorbing layers," *Opt. Commun.* **283**(23), 4810–4815 (2010).
6. W. R. Zipfel, R. M. Williams, and W. W. Webb, "Nonlinear magic: multiphoton microscopy in the biosciences," *Nat. Biotechnol.* **21**(11), 1369–1377 (2003).
7. F. Aptel, N. Olivier, A. Deniset-Besseau, J.-M. Legeais, K. Plamann, M.-C. Schanne-Klein, and E. Beaurepaire, "Multimodal nonlinear imaging of the human cornea," *Invest. Ophthalmol. Vis. Sci.* **51**(5), 2459–2465 (2010).
8. M. Zimmerley, R. Younger, T. Valenton, D. C. Oertel, J. L. Ward, and E. O. Potma, "Molecular orientation in dry and hydrated cellulose fibers: A coherent anti-Stokes Raman scattering microscopy study," *J. Phys. Chem. B* **114**(31), 10200–10208 (2010).
9. G. Filippidis, M. Massaouti, A. Selimis, E. Gualda, J.-M. Manceau, and S. Tzortzakis, "Nonlinear imaging and THz diagnostic tools in the service of cultural heritage," *Appl. Phys. A Mater. Sci. Process.* **106**(2), 257–263 (2012).

10. I. G. Cormack, P. Loza-Alvarez, L. Sarrado, S. Tomás, I. Amat-Roldan, L. Torner, D. Artigas, J. Guitart, J. Pera, and J. Ros, "Lost writing uncovered by laser two-photon fluorescence provides a *terminus post quem* for Roman colonization of *Hispania Citerior*," *J. Archaeol. Sci.* **34**(10), 1594–1600 (2007).
11. G. Filippidis, E. J. Gualda, K. Melessanaki, and C. Fotakis, "Nonlinear imaging microscopy techniques as diagnostic tools for art conservation studies," *Opt. Lett.* **33**(3), 240–242 (2008).
12. G. Filippidis, K. Melessanaki, and C. Fotakis, "Second and third harmonic generation measurements of glues used for lining textile supports of painted artworks," *Anal. Bioanal. Chem.* **395**(7), 2161–2166 (2009).
13. P. Samineni, A. deCruz, T. E. Villafañá, W. S. Warren, and M. C. Fischer, "Pump-probe imaging of historical pigments used in paintings," *Opt. Lett.* **37**(8), 1310–1312 (2012).
14. G. Latour, I. Gusachenko, L. Kowalczyk, I. Lamarre, and M. C. Schanne-Klein, "In vivo structural imaging of the cornea by polarization-resolved second harmonic microscopy," *Biomed. Opt. Express* **3**(1), 1–15 (2012).
15. G. Cox, N. Moreno, and J. Feijó, "Second-harmonic imaging of plant polysaccharides," *J. Biomed. Opt.* **10**(2), 024013 (2005).
16. R. M. Brown, Jr., A. C. Millard, and P. J. Campagnola, "Macromolecular structure of cellulose studied by second-harmonic generation imaging microscopy," *Opt. Lett.* **28**(22), 2207–2209 (2003).
17. I. Vazquez-Cooz and R. W. Meyer, "Fundamental differences between two fiber types in *Acer*," *IAWA J.* **29**, 129–141 (2008).
18. D. Débarre, N. Olivier, and E. Beaurepaire, "Signal epidetection in third-harmonic generation microscopy of turbid media," *Opt. Express* **15**(14), 8913–8924 (2007).
19. Y. Marubashi, T. Higashi, S. Hirakawa, S. Tani, T. Erata, P. Takai, and J. Kawamata, "Second harmonic generation measurements for biomacromolecules: celluloses," *Opt. Rev.* **11**(6), 385–387 (2004).
20. J. Hafren, D. Muhic, H. C. Gerritsen, and A. N. Bader, "Two-photon autofluorescence spectral imaging applied to probe process-effects in thermomechanical pulp refining," *Nordic Pulp Paper Res. J.* **26**(04), 3372–3379 (2011).
21. Y. Zeng, B. Saar, M. Friedrich, F. Chen, Y.-S. Liu, R. Dixon, M. Himmel, X. Xie, and S.-Y. Ding, "Imaging lignin-downregulated alfalfa using coherent anti-Stokes Raman scattering microscopy," *BioEnergy Res.* **3**(3), 272–277 (2010).
22. B.-C. Chen, J. Sung, and S.-H. Lim, "Chemical imaging with frequency modulation coherent anti-Stokes Raman scattering microscopy at the vibrational fingerprint region," *J. Phys. Chem. B* **114**(50), 16871–16880 (2010).
23. O. Nadiarnykh, R. B. Lacombe, P. J. Campagnola, and W. A. Mohler, "Coherent and incoherent SHG in fibrillar cellulose matrices," *Opt. Express* **15**(6), 3348–3360 (2007).
24. I. Gusachenko, V. Tran, Y. G. Houssen, J.-M. Allain, and M.-C. Schanne-Klein, "Polarization-resolved second-harmonic generation in tendon upon mechanical stretching," *Biophys. J.* **102**(9), 2220–2229 (2012).
25. R. Hori, M. Müller, U. Watanabe, H. C. Lichtenegger, P. Fratzl, and J. Sugiyama, "The importance of seasonal differences in the cellulose microfibril angle in softwoods in determining acoustic properties," *J. Mater. Sci.* **37**(20), 4279–4284 (2002).
26. S. J. Eichhorn, R. J. Young, and G. R. Davies, "Modeling crystal and molecular deformation in regenerated cellulose fibers," *Biomacromolecules* **6**(1), 507–513 (2005).
27. R. W. Boyd, *Nonlinear Optics, third edition* (Elsevier, 2008).
28. E. Martin, N. Sonoda, and A. R. Duval, "Contribution à l'étude des préparations blanches des tableaux italiens sur bois," *Stud. Conserv.* **37**(2), 82–92 (1992).
29. M.-J. Benquerença, N. F. C. Mendes, E. Castellucci, V. M. F. Gaspar, and F. P. S. C. Gil, "Micro-Raman spectroscopy analysis of 16th century Portuguese Ferreirim Masters oil paintings," *J. Raman Spectrosc.* **40**, 2135–2143 (2009).
30. F. Rosi, A. Daveri, B. Doherty, S. Nazzareni, B. G. Brunetti, A. Sgamellotti, and C. Miliani, "On the use of overtone and combination bands for the analysis of the $\text{CaSO}_4\text{-H}_2\text{O}$ system by mid-infrared reflection spectroscopy," *Appl. Spectrosc.* **64**(8), 956–963 (2010).
31. A.-M. Bakr, T. Kawiak, M. Pawlikowski, and Z. Sawlowicz, "Characterisation of 15th century red and black pastes used for wall decoration in the Qijmas El-Eshaqi mosque (Cairo, Egypt)" *J. Cult. Herit.* **6**(4), 351–356 (2005).
32. A. Claro, M. J. Melo, S. Schäfer, J. S. S. de Melo, F. Pina, K. J. van den Berg, and A. Burnstock, "The use of microspectrofluorimetry for the characterization of lake pigments," *Talanta* **74**(4), 922–929 (2008).
33. A. Nevin, D. Anglos, S. Cather, and A. Burnstock, "The influence of visible light and inorganic pigments on fluorescence excitation emission spectra of egg-, casein- and collagen-based painting media," *Appl. Phys. A Mater. Sci. Process.* **92**(1), 69–76 (2008).
34. M. Thoury, J.-P. Echard, M. Réfrégiers, B. Berrie, A. Nevin, F. Jammé, and L. Bertrand, "Synchrotron UV-visible multispectral luminescence microimaging of historical samples," *Anal. Chem.* **83**(5), 1737–1745 (2011).
35. J. Kirby and R. White, "The identification of red lake pigment dyestuffs and a discussion of their use," *The National Gallery Technical Bulletin* **17**, 56–80 (1996).
36. J.-P. Echard, L. Bertrand, A. von Bohlen, A.-S. Le Hô, C. Paris, L. Bellot-Gurlet, B. Soulier, A. Lattuat-Derieux, S. Thao, L. Robinet, B. Lavédrine, and S. Vaiedelich, "The nature of the extraordinary finish of Stradivari's instruments," *Angew. Chem. Int. Ed. Engl.* **49**(1), 197–201 (2010).
37. C. Clementi, B. Doherty, P. Gentili, C. Miliani, A. Romani, B. G. Brunetti, and A. Sgamellotti, "Vibrational and electronic properties of painting lakes," *Appl. Phys., A Mater. Sci. Process.* **92**(1), 25–33 (2008).
38. M. Thoury, M. Elias, J. M. Frigerio, and C. Barthou, "Nondestructive varnish identification by ultraviolet fluorescence spectroscopy," *Appl. Spectrosc.* **61**(12), 1275–1282 (2007).

39. A. Nevin, J.-P. Echard, M. Thoury, D. Comelli, G. Valentini, and R. Cubeddu, "Excitation emission and time-resolved fluorescence spectroscopy of selected varnishes used in historical musical instruments," *Talanta* **80**(1), 286–293 (2009).
40. A. Pena, M. Strupler, T. Boulesteix, and M. Schanne-Klein, "Spectroscopic analysis of keratin endogenous signal for skin multiphoton microscopy," *Opt. Express* **13**(16), 6268–6274 (2005).
-

1. Introduction

Characterization of coatings is of the utmost importance for the understanding and conservation of artworks – easel paintings, sculptures, etc. – and more generally of cultural heritage artifacts – furniture, musical instruments, etc. In order to give a specific appearance to the pieces they produced, artists and craftsmen developed elaborate painting and finishing techniques, mostly based on multilayer coatings. These layers are named ground or preparation layer, paint layers, glaze or varnish depending on their function or their location in the stratigraphy, and each of them may have a specific composition. The organic film-making materials can be of animal origin (collagen derivatives from cartilage, bones, and skin, i.e. animal glues, as well as albumin or casein) or vegetal origin (oils, resins, gums). They may also contain a wide range of powdered inorganic fillers or pigments. For art historians, curators, conservators and conservation scientists, the chemical and structural characterization of the different layers, or coating stratigraphy, represents valuable data to determine the materials and techniques used by the artists or craftsmen to elaborate their work.

Traditional and still commonly used examination of coatings involves sampling of the coating, preparation of polished cross sections and characterization by techniques such as reflected light and UV-visible epiluminescence microscopy, scanning electron microscopy coupled to energy-dispersive X-ray spectroscopy (EDX), laser-induced breakdown spectroscopy (LIBS), micro-IR imaging spectroscopy, micro-Raman spectroscopy or micro-imaging luminescence spectroscopy. Investigation of cultural heritage artifacts would however strongly benefit from *in situ* and non-destructive techniques overcoming the limitations of conventional analysis tools and providing the following key information:

- (i) determination of the number of layers, their respective thickness and surface/interface topography, with a description of cracks in underlayers,
- (ii) localization, concentration, shape and orientation of particles,
- (iii) optical properties (absorption, diffusion, color, luminescence) of each component of the various layers: binding media and particles,
- (iv) chemical characterization of each component and identification of the materials.

Recently, alternative techniques have been developed to fulfill these requirements. Confocal Raman microscopy advantageously provides three-dimensional (3D) images with chemical selectivity, but it is a quite slow technique, in practice limited to two-dimensional (2D) images in scattering media [1]. Optical Coherence Tomography (OCT) is based on low-coherence interferometry and provides 3D structural imaging based on the spatial variation of the refractive index. This technique is today well-established for the research on cultural heritage artifacts [2, 3]. However, despite recent advances into spectral selectivity and spectroscopy [4, 5], OCT still lacks specificity to assess the nature of materials used since any scattering or reflecting particles or interfaces within the sample is detected. Moreover, in scattering media such as paint layers, images are blurred due to multiple scattering events.

Multiphoton microscopy (MPM), also called nonlinear optical microscopy, is an attractive alternative method for investigating cultural heritage artifacts. This technique has been developed for biomedical imaging and is now widely used in that field. It is based on the nonlinear optical interaction between a laser beam and the studied material [6]. This interaction is confined to the focal volume where the intensity is large enough to induce a nonlinear response of the sample. It leads to so-called optical sectioning, which provides intrinsic 3D resolution at the micrometer scale. The excitation wavelength is usually in the

near-infrared range, typically between 700 and 1000 nm, improving the penetration depth due to weaker scattering in this spectral range, and limiting possible photodamage. A key advantage of MPM is the possibility to combine several modes of contrast, mainly two- or three-photon excited fluorescence (2PEF, 3PEF) from fluorophores, second harmonic generation (SHG) from non centrosymmetric structures and third harmonic generation (THG) from interfaces [7]. All these signals are emitted at different wavelengths and can be simultaneously recorded in different spectral detection channels to obtain multimodal images. Moreover, coherent anti-Stokes Raman scattering (CARS) microscopy provides chemical specificity [8], although this nonlinear vibrational technique requires an elaborated setup for pump and Stokes excitations.

Despite these advantages, few MPM studies have been performed on cultural heritage artifacts [9]. 2PEF was used to recover lost writing on a Roman amphora [10] and 3PEF was used to determine the stratigraphy on model coatings [11]. The only application of SHG was the identification of a starch-containing layer in a model coating through depth intensity profiles [12]. THG was used to determine interfaces in multilayered samples by recording intensity depth profiles in a transdetection configuration [11, 12]. Nevertheless, THG signals could not be detected in the backward direction, preventing any measurement on a bulk sample. Finally, pump-probe imaging was recently shown to enable identification of historical pigments from their chemical signatures [13]. Most of these MPM studies were performed in model samples.

Here, we present combined backward-detected 2PEF/SHG images of model samples and of a violin and attribute these two types of signals to specific components in the samples. To that end, we first analyze separately various coatings and wood shavings, and we then study a multilayer model sample that mimics multilayered systems encountered in historical artifacts. This MPM study therefore represents a major step ahead toward the fulfilling of the key requirements listed above. It shows that 2PEF/SHG imaging is a non-destructive and contactless technique for 3D specific and contrasted mapping of various key components of historical artifacts with a micrometer scale resolution. Finally, the analysis of the varnish on a century-old violin demonstrates the potential of this technique for *in situ* investigation of artworks.

2. Materials and methods

2.1. Multiphoton microscopy setup

A custom-built multiphoton upright microscope was used to perform these experiments as previously described [14] (Fig. 1(a)). The laser source was a femtosecond titanium:sapphire laser (Tsunami, SpectraPhysics) tuned to 860 nm and scanned within the sample to record pixel-wise images. The incident beam was circularly polarized using a quarter waveplate to image all components in a similar way regardless of their orientation in the focal plane [14]. A high numerical aperture air objective (20x, NA 0.75, Olympus) was used to achieve approximately 0.45 μm lateral by 1.6 μm axial resolutions near the sample surface. 2PEF signals were backward detected either with no spectral selection (GG455 high-pass filter, Schott), or in two distinct spectral bands, respectively, around 485 nm (485/70 bandpass filter, Semrock) and above 590 nm (RG590 high-pass filter, Schott) (see Fig. 1(b)). SHG signals were backward detected at half the incident excitation wavelength (427/10 interferential filter, Semrock). Forward SHG signals were also recorded in the case of transparent thin samples. Suitable filters were used to reject the excitation laser beam (FF01-680/SP and FF01-720SP short-pass filters, Semrock). Both 2PEF and SHG signals were detected using photon-counting photomultiplier tubes (P25PC, Electron Tubes). In all the figures, 2PEF and SHG signals are represented in red and green, respectively.

The recorded image size was 480 x 480 pixels with 0.8 μm pixel size, corresponding to a 380 x 380 μm^2 field of view. 3D data were recorded by axially shifting the objective mounted on a translation stage with 0.5 μm axial steps. The acquisition pixel rate was 200 kHz, or

approximately one image per second. Laser power at the objective focus was 8 to 20 mW, without any observable damage in the studied samples.

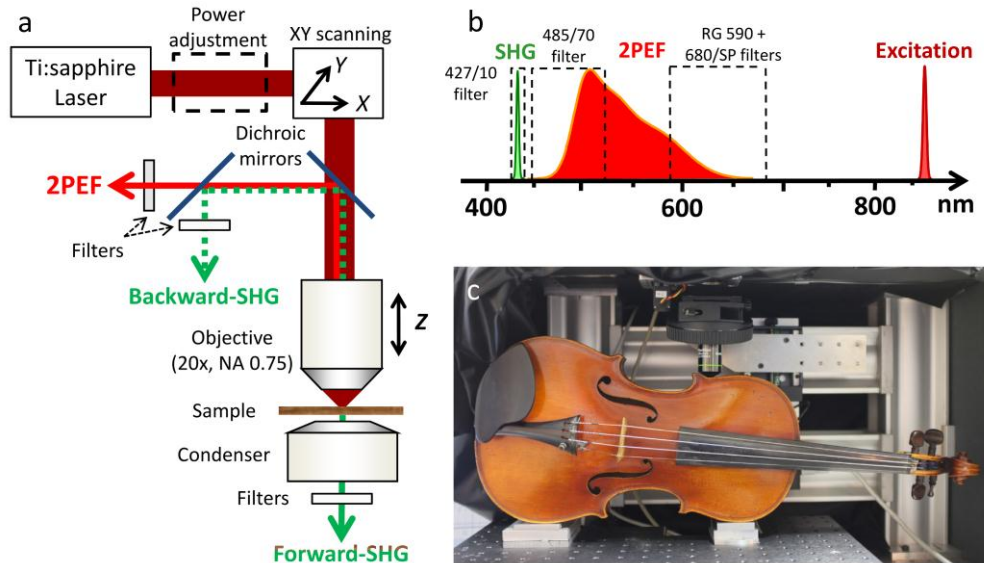


Fig. 1. Experimental setup. (a) Scheme of the multiphoton microscope with air objective (20x, NA 0.75) and three detection channels with well-suited filters for the different modes of contrast: 2PEF and backward-SHG for non-transparent and bulky samples, and forward SHG for thin samples. (b) Detection spectral ranges for excitation at 860 nm: half the excitation wavelength for SHG and two spectral bands for 2PEF. (c) Experimental setup adapted for *in situ* analysis of a historical violin.

2.2. Samples

We investigated the 2PEF and SHG properties of a set of compounds that were widely used as artists' materials. Figure 2 summarizes the composition of these model samples, along with the observed signals.

Maple wood (*Acer pseudoplatanus*) is an important structural and finishing material used in furniture, musical instruments and decorative objects. For this study, we first imaged thin wood shavings, cut along conventional wood planes, and then in bulky samples finished with different coatings. Note that wood shavings were flattened between two glass coverslips and imaged using a water-immersion objective (20x, NA 0.95, Olympus).

Various model paint and glaze layers, a few tenths of micrometer thick, were prepared using film-making materials, pigments and mineral fillers. Gelatin-based glue (GT58, Laverdure, Paris) and sandarac resin from restoration materials (Musée de la musique laboratory) were prepared as dried films. One red lake pigment, cochineal on alumina (prepared at the Musée de la musique laboratory according to a historical recipe), and one filler, plaster of Paris (Staturoc, Rougier & Plé, Paris) were incorporated in these binders: plaster in gelatin film, cochineal lake pigment in gelatin film and in sandarac film. A multi-layered system was also prepared in the following way: wood (substrate), plaster in gelatin (lower layer), cochineal lake pigment in sandarac (upper layer) (see scheme in Fig. 2).

Finally, the coating of a violin (Neuner & Hornsteiner, Mittenwald, Germany, early 20th century, private collection) was analyzed *in situ*. For these experiments, the sample stage and forward-SHG detection module were removed to have enough space to put the instrument at the objective focus (see picture in Fig. 1(c)).





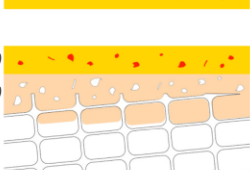
Samples		Emitted multiphoton signals	
		2PEF	SHG
Wood (<i>Acer</i>) (thickness $\approx 30\ \mu\text{m}$)		lignin	cellulose
Gelatin-based film containing plaster (thickness $\approx 30\ \mu\text{m}$)		No signal	plaster
Gelatin-based film containing cochineal lake (thickness $\approx 27\ \mu\text{m}$)		cochineal lake (above 590 nm)	No signal
Sandarac film containing cochineal lake (thickness $\approx 23\ \mu\text{m}$)		cochineal lake (above 590 nm) sandarac (around 485 nm)	No signal
Multilayer model sample	 L1 ($\sim 25\ \mu\text{m}$) L2 ($\sim 20\ \mu\text{m}$) L3	cochineal lake (above 590 nm) sandarac (around 485 nm) lignin	plaster cellulose

Fig. 2. Model samples and nonlinear signals collected. Description of the model samples (composition, thickness and scheme) and origin of the corresponding 2PEF and SHG signals.

3. Results

3.1. Wood

MPM was first performed in a thin shaving (about $30\ \mu\text{m}$ thick) of *Acer pseudoplatanus* wood. 2PEF images (using high-pass GG455 filter) revealed the well-known wood structure, specifically the wood fibers (see the lower part of Fig. 3(a)) and groups of medullary rays (see the top part of Fig. 3(a)). These 2PEF signals are emitted by lignin in wood fibers as described previously [15]. SHG signals were detected both in forward and backward directions (Fig. 3(b) and 3(c) respectively) with similar signal intensities (forward/backward ≈ 0.6 after correction by the channel sensitivities). These signals have been reported to be specific to crystalline cellulose [15, 16]. 3D reconstructions were also performed (Fig. 3(e) and Media 1). SHG and 2PEF images thus provided complementary information by revealing different components of the wood fibers.

3.2. Gelatin-based film containing plaster

No fluorescence was detected from the $30\ \mu\text{m}$ thick gelatin-based film (as detailed in part 3.3), whereas plaster radiated strong SHG signals both in forward and backward directions. Figures 4(a) and 4(b) display an optically sectioned slice $20\ \mu\text{m}$ deep within the sample. The same area was observed using transmitted light microscopy (TLM, see Fig. 4(c)) and plaster particles were easily recognized. Comparison of SHG and TLM images showed that only the particles contained within the focal plane were observed in MPM, highlighting the optical sectioning performed by this technique. Nevertheless, it was possible to visualize all the particles contained within the coating using SHG microscopy by summing all the images recorded at increasing depth, as shown in Fig. 4(d) and 4(e) for forward and backward signals respectively. These z-projections were similar to the TLM view, confirming that all the plaster particles were SHG emitters. Finally, 3D renderings were generated from the same SHG image stack and revealed the 3D distribution of plaster particles (see Fig. 4(f)).

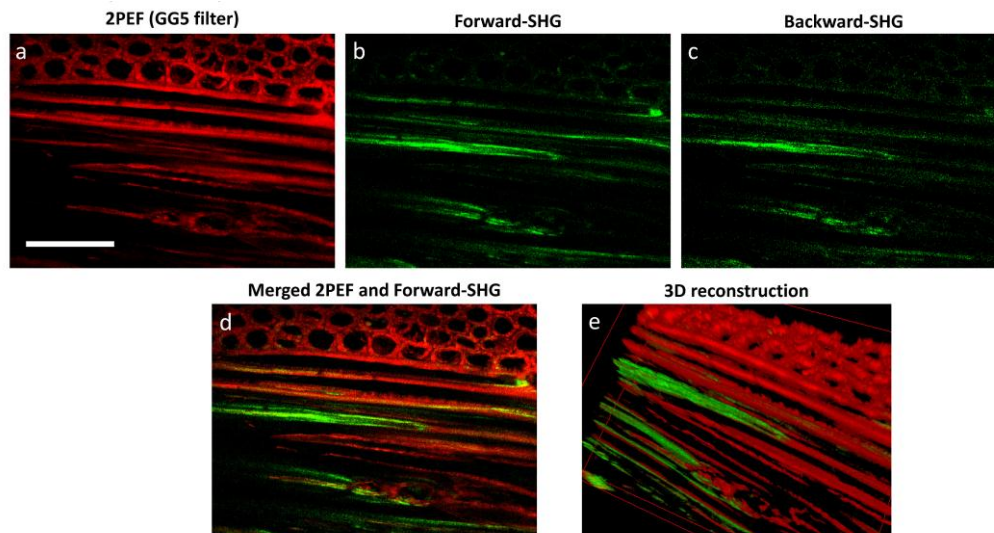


Fig. 3. MPM imaging of a thin wood shaving. (a) 2PEF signals from lignin. (b) Forward and (c) backward SHG signals from crystalline cellulose. (d) Merged 2PEF (red) and forward-SHG (green) image and (e) 3D reconstruction of the same region (see also [Media 1](#)). Scale bar: 100 μm .

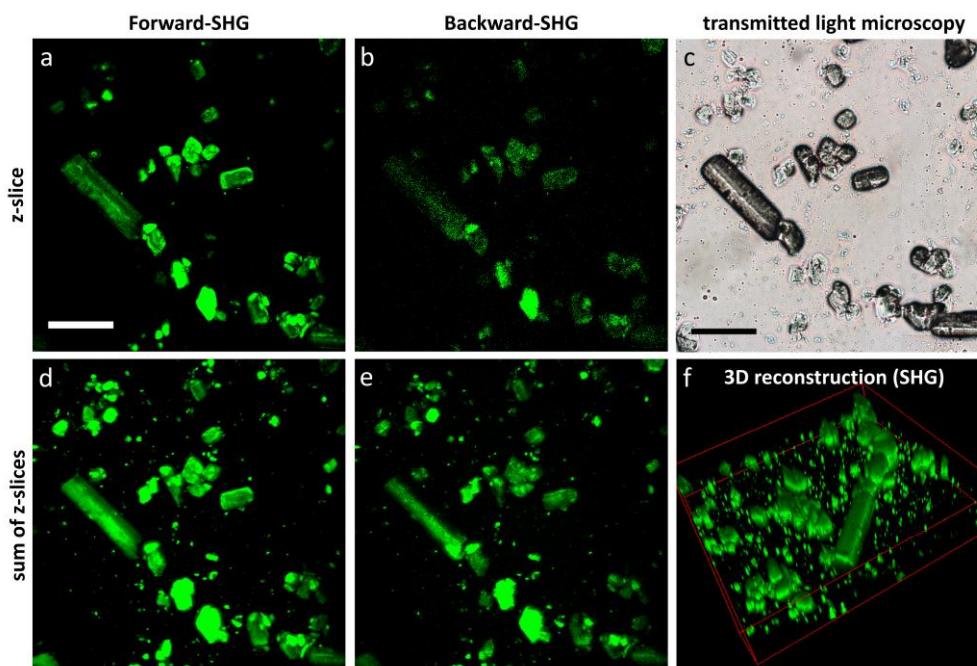


Fig. 4. SHG and TLM imaging of plaster particles dispersed in gelatin-based film. (a, d) Forward and (b, e) backward SHG images compared to (c) TLM image in the same area. (a-b) Optically sectioned SHG images at depth $z = 20 \mu\text{m}$ within the sample and (d-e) sum of 120 SHG images in a $40 \mu\text{m}$ -thick z-stack, providing projected images similar to the TLM one. (f) 3D reconstruction of the forward SHG image z-stack that allows the spatial localization of the plaster particles within the layer. Scale bar: $100 \mu\text{m}$.

3.3. Gelatin-based and sandarac films containing cochineal lake pigments

Cochineal lake pigments in a 27 μm thick gelatin-based film and in a 30 μm thick sandarac film (Fig. 5(a-c) and Fig. 5(d-f) respectively) were observed using two distinct 2PEF spectral bands, respectively around 485 nm (Fig. 5(a) and 5(d)) and above 590 nm (Fig. 5(b) and 5(e)). Around 485 nm, there was no fluorescence from the gelatin-based film (Fig. 5(a)), as already observed in the previous gelatin-based film containing plaster, whereas sandarac emitted strong 2PEF signals (Fig. 5(d)). In this case, the cochineal lake particles were observed in negative contrast due to the absence of 2PEF signals from these particles in this spectral band. In the second spectral band, above 590 nm, pigment particles exhibited intense 2PEF signals, strongly contrasting with the weak or null emission of the binder (Fig. 5(b) and 5(e)). This observation was confirmed by comparison to TLM (Fig. 5(c) and 5(f)). The shapes of the different particles were recognized; however, as in the plaster imaging, only few pigment particles were observed per image due to the optical sectioning of MPM. It therefore enabled 3D localization of the pigments within the binding layer with a micrometer spatial resolution. Note that no SHG signal was observed from these components.

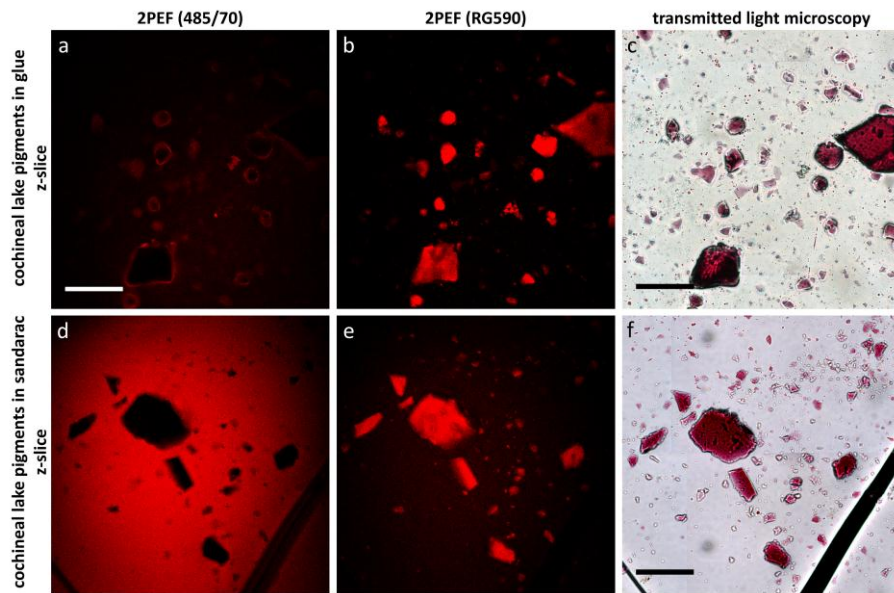


Fig. 5. 2PEF and TLM imaging of cochineal lake pigments dispersed in gelatin-based glue and sandarac films. Cochineal lake pigments (a-c) in gelatin-based glue film and (d-f) in sandarac film observed by (a-b, d-e) 2PEF microscopy and compared to (c, f) TLM. 2PEF signals were detected in two spectral bands: (a, d) around 485 nm and (d, e) above 590 nm. Scale bar: 100 μm .

3.4. Model multilayered coating

MPM imaging of the model multilayered sample revealed different structures at different depths, distinguished by collecting two distinct 2PEF spectral bands (around 485 nm in Fig. 6(a), 6(d) and 6(g) and above 590 nm in Fig. 6(b), 6(e) and 6(h)) and backward SHG signals simultaneously (Fig. 6(c), 6(f) and 6(i)) (see [Media 2](#) for a z-stack of the three detection channels). The first layer from the surface, which was composed of cochineal lake pigments in sandarac, exhibited spectrally distinct 2PEF signals from the binding medium at 485 nm and from the pigment particles at longer wavelengths (Fig. 6(a-c)). Images from the second layer composed of plaster in gelatin-based glue were detected by focusing the laser beam deeper in the sample (Fig. 6(d-f)). As expected, there was no fluorescence, neither from the binding medium nor from the plaster particles, whereas strong SHG signals were collected

from the plaster particles. Finally, MPM imaging revealed the wood features under the two previous layers by combining 2PEF signals from the lignin and SHG signals from cellulose (Fig. 6(g-i)).

Axial reconstructions were performed from the collected data stacks (Fig. 6(j) and 6(k)) to characterize the layered system. The contributions of sandarac (2PEF at 485 nm), cochineal lake pigments (2PEF above 590 nm) and plaster particles (SHG) were visible at different depths. The wood signals were also observed in the bottom part of these reconstructions. Using these views, we were able to determine the thickness of each layer without any sampling of the model stratigraphy: around 25 μm for the fluorescent sandarac layer and 20 μm for the glue layer. 3D reconstructions were also performed and allowed spatial localization and identification of the different particles by use of their MPM response (Fig. 6(l) and [Media 3](#)). It is worth noting that both 2PEF and SHG signals were detected up to a depth of 80 μm , through two different scattering layers. SHG/2PEF merged images of the *Acer* wood, underneath the multi-layer coating, still revealed quite sharp features (Fig. 6(m)) as in wood shavings alone. SHG signals from cellulose were only radiated by thin structures in the wood cell walls, whereas 2PEF signals from lignin appeared in larger areas. This allowed the visualization of fine wood structures such as bordered pits (see inset Fig. 6(m)) [17].

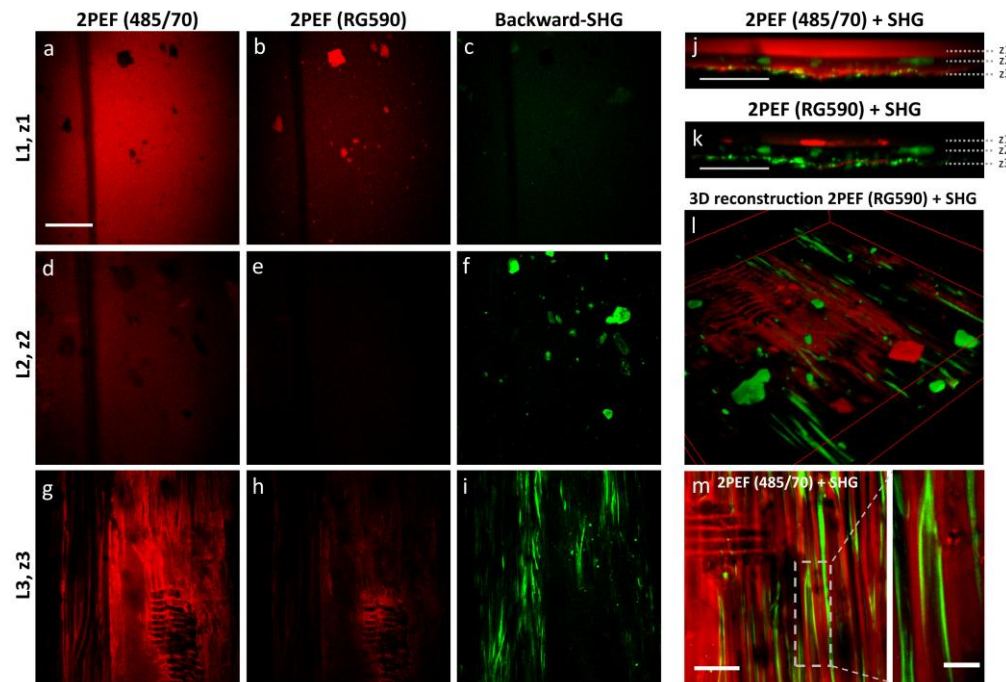


Fig. 6. Multiphoton microscopy of a multilayered coating system on wood. 2PEF (a, d, g) around 485 nm and (b, e, h) above 590 nm and (c, f, i) SHG imaging at three different depths ($z1 = 27 \mu\text{m}$, $z2 = 43 \mu\text{m}$ and $z3 = 60 \mu\text{m}$) ([Media 2](#)). Scale bar: 100 μm . (j, k) Axial reconstruction of MPM images combining SHG (green), revealing plaster particles and wood cellulose, and 2PEF (red) in two spectral bands: (j) around 485 nm, revealing the sandarac film and the wood lignin and (k) above 590 nm, revealing cochineal lake pigments. Scale bar: 100 μm . (l) 3D reconstruction allowing identification and spatial localization of the particles. See also [Media 3](#) in another region. (m) 2PEF (red, around 485 nm) and SHG (green) imaging of wood at 50 μm depth, below the varnish coatings. Scale bar: 50 μm . Inset: zoomed view of a few wood fibers that enables the spatial localization of lignin and cellulose. Scale bar: 15 μm .

3.5. Violin

In situ MPM was performed on a historical violin as shown in Fig. 1(c). Two areas were studied: an area bearing a quite thick multilayer coating on the side of the soundbox (upper rib on the treble side), and a locally damaged area, without any coating, on the head (see scheme in Fig. 7(l)). 2PEF images collected at various depths in the coated area (Fig. 7(a-f) and Media 4) illustrate the advantages of a setup enabling optical sectioning compared to conventional fluorescence microscopy (Fig. 7(g-i)). At a depth of 9 μm , 2PEF signals collected in the two spectral ranges under study (around 485 nm in Fig. 7(c), and above 590 nm in Fig. 7(d)) were distinctly different. The cracks were clearly revealed in positive contrast in the 485 nm spectral range, with few particles evidenced in negative contrast. In the spectral range above 590 nm, the cracks were barely discernable in a continuous fluorescence background, while much more particles were evidenced in negative contrast. Deeper in the violin, 2PEF imaging revealed the structure of the wood (Fig. 7(e-f)), whereas *in situ* conventional white light and fluorescence microscopies gave blurry images in the same area. The wood structure was also observed *in situ* on the head of the violin with damaged coating. 2PEF and SHG signals from the wood fibers were detected as depicted in Fig. 7(j-k).

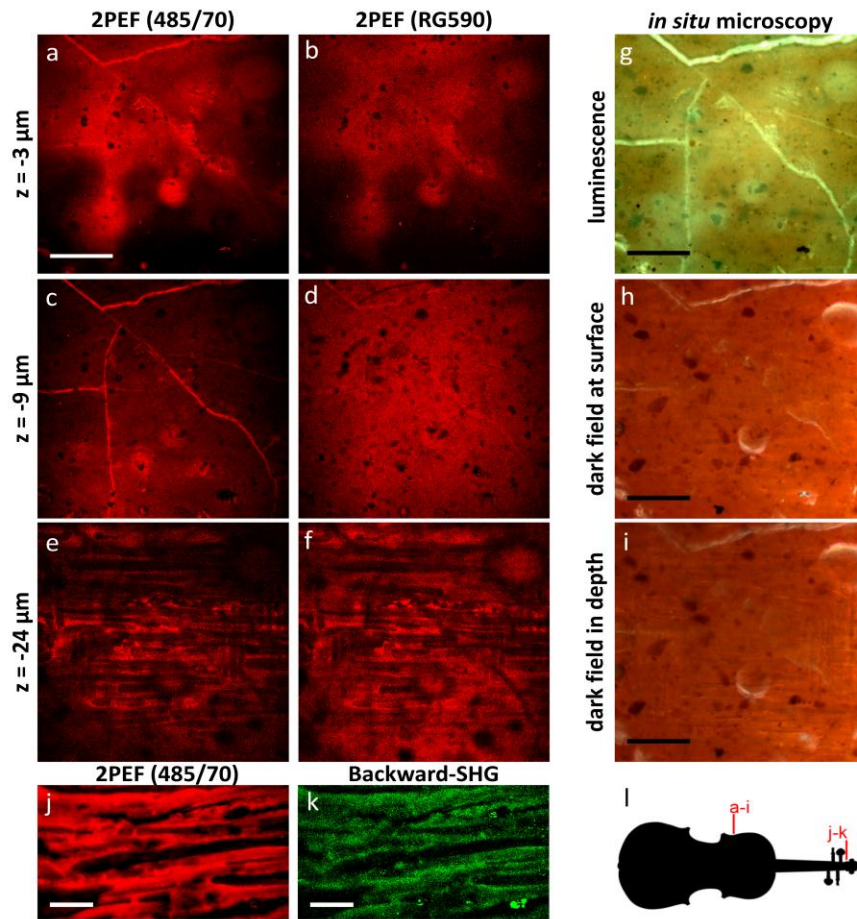


Fig. 7. *In situ* observation of a historical violin by multiphoton microscopy. Observations were performed in two areas: (a-i) the side of the soundbox and (j-k) the head of the violin as represented in the scheme (l). Images of the side area by 2PEF microscopy (a, c, e) around 485 nm and (b, d, f) above 590 nm (Media 4) and by (g) luminescence and (h-i) dark field microscopy. 2PEF microscopy was performed at three different depths: (a-b) 3 μm , (c-d) 9 μm and (e-f) 24 μm . Scale bar: 100 μm . (j) 2PEF and (k) SHG images of wood on the head. Scale bar: 30 μm .

4. Discussion and perspectives

4.1. Multiphoton imaging for the study of cultural heritage artifacts

In situ 3D imaging techniques provide key information for the study of cultural heritage artifacts, which explains the recent development of OCT in that field [3]. Nevertheless, few OCT setups reach micrometer scale resolution allowing particle imaging and wood structure characterization [2]. Moreover, this technique lacks chemical specificity, so that complementary studies using invasive techniques are usually required to identify the materials. In this work, we have demonstrated that 2PEF/SHG microscopy overcomes these limitations by providing specific and contrasted 3D structural images, while preserving a low invasive and user-friendly setup.

We showed that well-resolved and well-contrasted MPM images can be obtained with an air objective rather than the water-immersion objectives commonly used in the biomedical field. This is crucial because many materials encountered in artworks are liquid-sensitive and sometimes porous. Moreover, our MPM images were recorded in the backward direction, which enables the analysis of samples of any thickness. This backward-configuration is usual for 2PEF signals that are emitted isotropically, whereas SHG radiation is generally more efficient in the forward direction due to phase-matching conditions. Nevertheless, as in other coherent microscopies, SHG signals can be recorded in the backward direction when SHG backward radiation is enhanced by specific spatial structures or when forward-radiated SHG signals are backscattered in thick scattering samples [18]. Practically, we showed that SHG signals from both cellulose and plaster can be backward detected, opening the way to *in situ* characterization. Finally, in our experimental conditions, with a power at the focal point below 20 mW, no damage has been observed in any of the studied model samples and violin. Nevertheless, modification could occur in light-sensitive materials after prolonged exposure. For further studies, the power threshold should be adapted to each sample depending on the absorption properties of the materials.

4.2. Multiphoton imaging of wood

MPM imaging of wood showed both 2PEF and SHG signals. SHG signals arise from crystalline cellulose as already reported [8, 15, 16]. Cellulose is composed of polysaccharidic chains that occur naturally in two forms I_α (triclinic, space group P1) and I_β (monoclinic, space group P2₁). These well-ordered molecular chains are organized to form microfibrils with typical diameter from 2 to 20 nm. This hierarchical ultrastructure and the parallel orientation of the molecular chains explain the emission of SHG signals [8, 15, 16, 19]. SHG signals, however, are not as strong as in starch because of the reverse orientation of glucose residues in the polysaccharidic chains, as discussed in [15].

Wood fluorescence is attributed to lignin [15, 17]. In this work, we observed 2PEF in the 450–520 nm spectral range (485/70 bandpass filter) upon excitation at 860 nm. This is in agreement with the spectroscopic fluorescence properties of lignin [20] and with previous observations using nonlinear excited fluorescence [21].

Combined SHG/2PEF microscopy thus allows simultaneous imaging of cellulose and lignin, two major components of wood, as reported previously in celery petiole [15]. Similar multimodal imaging has been demonstrated with CARS microscopy by using C=C vibration at 1600 cm⁻¹ as a lignin marker and C-O-C vibration at 1100 cm⁻¹ as a cellulose marker [22]. However, implementation of CARS microscopy is not as straightforward as SHG and 2PEF microscopies which require only one standard femtosecond laser beam. SHG/2PEF microscopy thus provides a simple means for 3D *in situ* mapping of wood cell walls at the sub-micrometer scale and should enable a better insight into their organization. It could be further improved by using an objective with higher numerical aperture to increase the lateral resolution, while fine wood structures such as bordered pits were already visible in the inset of Fig. 6(m). Another perspective is to implement polarization-resolved SHG imaging to determine the orientation of cellulose microfibrils [16, 23] and to gain insight into cellulose organization in cell walls. In a similar way, polarization-resolved CARS microscopy enabled

the determination of the molecular orientation in dry and hydrated cellulose fibers [8]. More generally, polarization-resolved approaches are sensitive to the distribution of orientations at the submicrometer scale, that is, below the optical resolution [14, 24]. Quantitative information could thus be obtained using this technique to compare different wood species or to study the effects of treatment or aging on wood microstructure.

It is worth noting that these microscopic properties are key parameters to better characterize the macroscopic mechanical properties of wood [25, 26]. A previous study based on Raman microscopy suggested changes at the molecular scale in zones of tension wood [1]. Determination of the relationship between the distribution of the cellulose and the wood mechanical properties would be of great interest to characterize wooden artifacts such as musical instruments, especially for their acoustic properties [25] or for the sensitivity of their mechanical constraints to micro-environmental changes.

4.3. SHG imaging of plaster

We showed that plaster, that is, calcium-sulfate particles, is a strong emitter of SHG signals which can be detected both in forward and backward directions. Note that there are 3 types of calcium-sulfate crystals depending on the water content: anhydrite CaSO_4 , hemihydrate $\text{CaSO}_4 \cdot 0.5\text{H}_2\text{O}$, also called bassanite, and dihydrate $\text{CaSO}_4 \cdot 2\text{H}_2\text{O}$, also called gypsum. Bassanite exhibits a pseudohexagonal monoclinic crystal structure that is non centrosymmetric, while anhydrite and gypsum are centrosymmetric crystals. Given that SHG vanishes for centrosymmetric materials, non zero SHG signals are only expected for bassanite particles [27]. Accordingly, complementary analysis by powder X-ray diffraction (XRD) showed that the plaster we used for the preparation of the samples was composed of very pure hemihydrate calcium sulfate.

The calcium sulfate-based preparation layers (gesso) encountered on Italian panel paintings before the 16th century are mostly anhydrite or gypsum. In some specific cases, bassanite, which is obtained by the heating of gypsum, has also been detected by X-ray diffraction, FTIR and Raman spectroscopy [28–30]. The relative ratios of these three compounds may be an indicator of the preparation process of gesso materials. It may also be used as an indicator of the degradation and transformation processes in mural decorations [31]. The ability to specifically image bassanite by SHG microscopy therefore opens new perspectives for conservation studies of the numerous works of art containing calcium-sulfate-based materials.

4.4. 2PEF spectral properties

Fluorescence properties of pigments and binding media have been widely studied using conventional setups based on linear excitation of these fluorophores. In particular, spectrally-resolved excitation and emission studies paved the way toward non-invasive and non-destructive identification of the components [32, 33]. However, most of the time, these techniques do not allow spatial characterization. To overcome this limitation, synchrotron multispectral luminescence studies have been recently reported and allowed mapping of spectral properties with micrometer scale resolution [34]. Nevertheless, user-friendly techniques are still needed that do not require access to a synchrotron source. In this paper, we demonstrated that 2PEF microscopy both provides 3D localization at micrometer scale and spectral properties of the fluorescence signals emitted by pigments and binding media, by use of a benchtop instrument.

Lake pigments have been widely used in easel paintings and have also been reported in the varnishes of 18th-century Italian violins by A. Stradivari [35, 36]. The coloring matter of these lakes consists of anthraquinone molecules extracted from various vegetal and animal species such as the cochineal *Dactylopius Coccus* Vast. which contains carminic acid, or the madder root *Rubia Tinctoria* which contains alizarin and purpurin. The color is stabilized with mineral treatments (for instance with potash alum), producing a complex between the coloring molecules and the mineral substrate according to processes already used by textile dyers in the Middle Ages. Most red lake pigments are fluorescent, with an emission in the

600-640 nm spectral range, the wavelength maximum depending on the origin of the dye and of the anthraquinone molecules in presence [37]. In accordance with these studies employing linear excitation, our 2PEF images showed that fluorescence of cochineal lake pigment is emitted in a spectral band above 590 nm.

Fluorescence spectra are usually broad in the visible range for protein-, resin- and oil-based paintings and varnish binding media [33, 38]. Typical fluorescence emission of sandarac upon linear excitation of 430 nm is a broad, bell-shaped spectrum, with a maximum emission around 500 nm and a FWHM of about 130 nm [39]. Accordingly, we observed that the sandarac 2PEF emission is intensely fluorescent beneath 590 nm when excited at 860 nm.

In this study, 2PEF emissions in two spectral bands were recorded sequentially by using two suitable spectral filters. Nevertheless, simultaneous acquisition of two or more spectral bands could be implemented in a straightforward way using appropriate dichroic mirrors and spectral filters to collect 2PEF signals on parallel detectors. Furthermore, emission and excitation 2PEF spectra could also be recorded as for biological fluorophores [40]. Such a spectroscopic analysis of pigments and binding media 2PEF signals would enable comparison with linear excitation and allow the optimization of the emission filters.

5. Conclusion

In this paper, we demonstrated key advantages of multiphoton microscopy for *in situ* characterization of historical artifacts. We obtained highly contrasted 3D images at the micrometer scale without any preparation or sampling of the artifacts. Specific signals were collected as a function of the chemical nature of the studied materials: SHG signals were obtained from cellulose and plaster and 2PEF signals were obtained from pigments such as cochineal lake pigments and binding media such as sandarac. Furthermore, we showed that spectral selection of 2PEF signals enables the discrimination of different pigments and binding media by taking advantage of their emission spectral ranges. We also showed that plaster particles composed of hemihydrate calcium sulphate, that is bassanite, exhibit SHG signals, as expected from theoretical considerations about material symmetry. Finally, *in situ* observations of a historical violin have been performed without any damage of the instrument. This study paves the way for numerous promising applications to the fields of ancient materials and conservation science, as well as, more generally, to the fields of coating materials and wood science.

Acknowledgments

The authors gratefully acknowledge Michael Palmer, National Gallery of Art, Washington DC USA, for performing the XRD analysis of the plaster of Paris and Max Zimmerley for fruitful discussion about multiphoton imaging of cellulose and for critical reading of the manuscript.